Supplement of Atmos. Meas. Tech., 19, 2737–2750, 2026
https://doi.org/10.5194/amt-19-2737-2026-supplement

Atmospheric Measurement Techniques
Open Access
EGU

Supplement of

Super-resolution localization and quantification of SO_2 emissions over India using TROPOMI observations

Yutao Chen et al.

Correspondence to: Yutao Chen (yutao.chen@knmi.nl) and Jieying Ding (jieying.ding@knmi.nl)

S1. The spreading effect led by divergence calculation

Since the data used for the divergence calculation, TROPOMI SO_2 measurements and 2D wind fields, are gridded rather than continuous, we calculate the SO_2 divergence using the second-order central difference method. The total divergence is a superposition of components in both the *x* and *y* directions; for simplicity, we present the calculation along the *x* direction only. Specifically, the SO_2 divergence of grid cell *i* in the *x* direction can be calculated as follows:

$$D_{x(i)} = \frac{F_{x(i+1)} - F_{x(i-1)}}{2\Delta x} \quad \text{(S1)}$$

$$F_{x(i+1)} = w_{x(i+1)} \cdot V_{(i+1)} \quad \text{(S2)}$$

$$F_{x(i-1)} = w_{x(i-1)} \cdot V_{(i-1)} \quad \text{(S3)}$$

$D_{x(i)}$ is the divergence in grid cell *i* calculated along the *x* direction. $F_{x(i)}$ denotes the flux of SO_2 in grid cell *i* along the *x* direction. ∇x is the resolution of the grid-scale. $w_{x(i)}$ represents the wind in grid cell *i* along *x* direction. V_i is SO_2 VCD in grid cell *i*. The total divergence for each grid cell equals the sum of the divergence along *x* and *y* directions.

There is a discretization in this divergence calculation leading to the spreading of the calculated point source emissions. Specifically, Eq. (1) can be rewritten as:

$$D_{x(i)} = \frac{1}{2}\left[\frac{(F_{x(i+1)} - F_{x(i)})}{\Delta x} + \frac{(F_{x(i)} - F_{x(i-1)})}{\Delta x}\right] \quad \text{(S4)}$$

This can further be expressed as:

$$D_{x(i)} = \frac{1}{2}[D_{RE(i)} + D_{LE(i)}], \quad \text{(S5)}$$

where $D_{RE(i)}$ and $D_{LE(i)}$ denotes the divergence at the right and left edges of grid cell *i*, respectively. Hence, the divergence of each grid cell can be viewed as a linear interpolation of the divergence in its surrounding regions. This causes the spreading of point source emissions. We use Eq. (S1) to calculate gridded SO_2 divergence at different spatial resolutions to determine the optimal resolution for emissions, which minimize both spreading effect and the noise level. The target spatial resolutions from coarse to fine are 0.1° × 0.1°, 0.05° × 0.05°, 0.025° × 0.025°, and 0.01° × 0.01°. Table S1 shows the six investigated divergence calculations using the mentioned resolutions and two calculation strategies. Either the divergence is first calculated on the TROPOMI pixels and then interpolated to the target resolution (option 1) or the SO_2 VCD is first interpolated to the target resolution, and then the divergence is calculated (option 2). The SO_2 emission results of these six cases are shown in Fig. S1.

Table S1. SO_2 emissions on different spatial scales

Case name	Method (1. Divergence calculation on TROPOMI pixels, 2. Divergence calculation on regular grid cells)	Spatial resolution
0.1°_Regular Grid	2	0.1° × 0.1°
0.05°_Regular Grid	2	0.05° × 0.05°
0.025°_Regular Grid	2	0.025° × 0.025°
0.025°_TROPOMI Pixel	1	0.025° × 0.025°
0.01°_Regular Grid	2	0.01° × 0.01°
0.01°_TROPOMI Pixel	1	0.01° × 0.01°

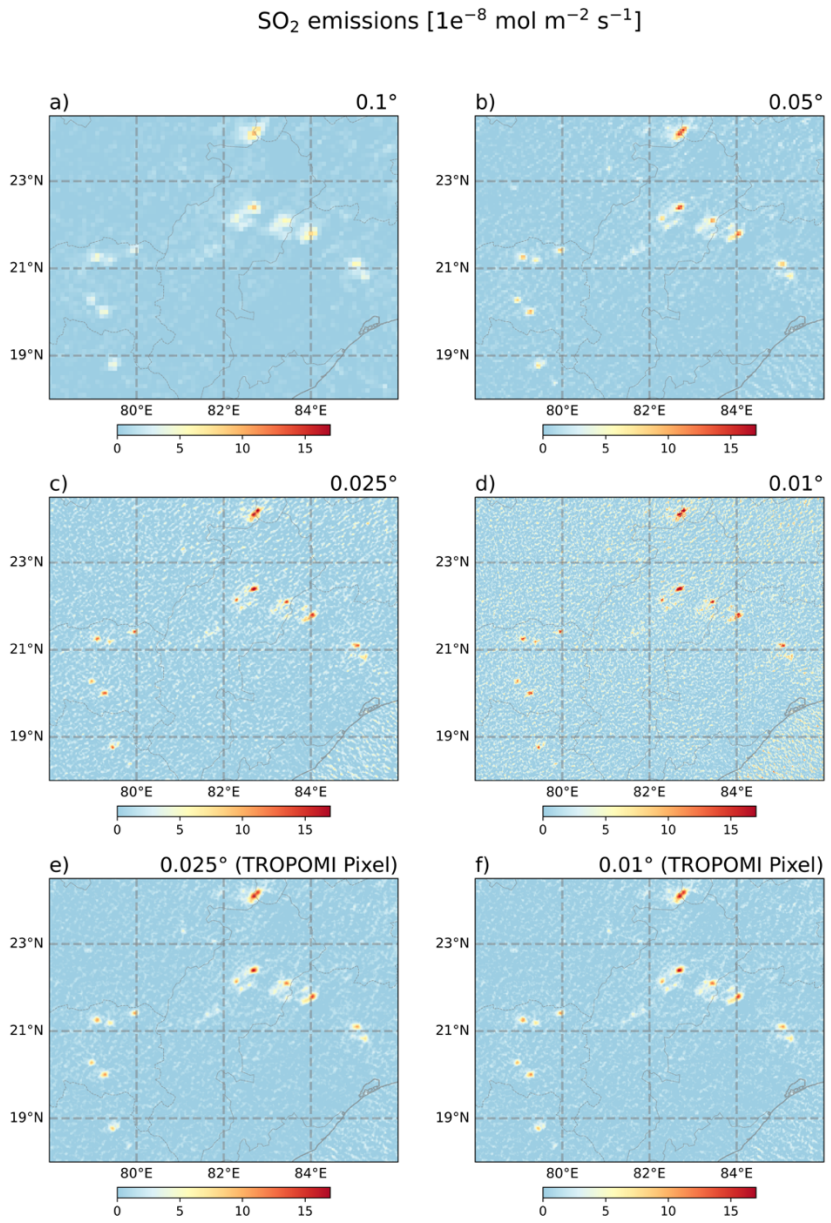

Figure S1. Annual mean SO_2 emissions during December 2022 to November 2023 on different spatial resolutions in a region of India with strong emission sources. The cases are shown for a) 0.1°_Regular Grid,

b) 0.05°_Regular Grid, c) 0.025°_Regular Grid, d) 0.01°_Regular Grid, e) 0.025°_TROPOMI Pixel, and f) 0.01°_TROPOMI Pixel.

In Fig. S1a-d, the SO_2 divergence is calculated directly on the regular grid in the target resolution. In Fig. S1a-c, as the grid resolution becomes finer, the SO_2 emission map shows more details, indicating the emission resolution also becomes finer. The higher grid resolution can reduce the spreading effect caused by the linear interpolation of divergence calculation and thus improve the emission resolution, while the noise level increases due to the finer resolution. However, when the grid resolution becomes finer than the TROPOMI pixel size, i.e. the grid resolution changes from 0.025° × 0.025° to 0.01° × 0.01° as shown in Fig.S1c and d, the improvement on emission resolution becomes minimal and the noise levels are still increasing. In this case, the TROPOMI pixel size becomes the limiting factor, and further increasing the grid resolution does not improve the effective emission resolution but increase the noise. When the resolution matches the resolution of Fig. S1c (0.025° × 0.025°) and d (0.01° × 0.01°), while the divergence is first calculated on the TROPOMI pixel as shown in Fig. 1e and f, the noise levels are efficiently reduced. The effective emission resolution between Fig. 1e and 1f are comparable, indicating that increasing the grid resolution no longer improves the effective emission resolution in this case. Nonetheless, some spreading of point-source emissions always remains, constrained either by the grid or the TROPOMI pixel size. In our study, we introduce a method to further improve the emission resolution on any given grid cell resolution. Fig. S1e and S1f show less noise compared to Fig. S1c and S1d, making it easier to distinguish point sources from the noise. Since the emission resolution in Fig. S1e (0.025°) and Fig. S1f (0.01°) are similar, we use the SO_2 emissions from Fig. S1e (0.025°) as the baseline in our study

S2. The Gaussian-shaped function to derive the spreading kernel $\boldsymbol{B}$

Each element in the spreading kernel is calculated based on the following function:

$$f(x) = e^{-\frac{x^2}{2\cdot\sigma^2}} \tag{S6}$$

With the known sigma, the variable x (in units of grid cells) is the distance from the center of the grid cell which contains the emission source. Specifically, when $x = 0$, it refers to the grid cell containing the point source itself. When $x = 1$, it refers to the distance to directly adjacent neighboring grid cells. When $x = \sqrt{2}$ (approximately 1.414), it refers to the distance to diagonally adjacent grid cells. Additional values of x represent distances to more distant grid cells, calculated according to their relative positions.

The spreading pattern $\boldsymbol{B'}$ is defined within a 9 × 9 grid cell area centered on the grid cell containing the point source and is derived from the Eq. S6. The spreading kernel $\boldsymbol{B}$, which is used to calculate the sharpening kernel, is the normalized form of $\boldsymbol{B'}$ and can be expressed as:

$$\boldsymbol{B} = \frac{\boldsymbol{B'}}{\sum_{i=-4}^{4}\sum_{i=-4}^{4}\boldsymbol{B'_{ij}}} \tag{S7}$$

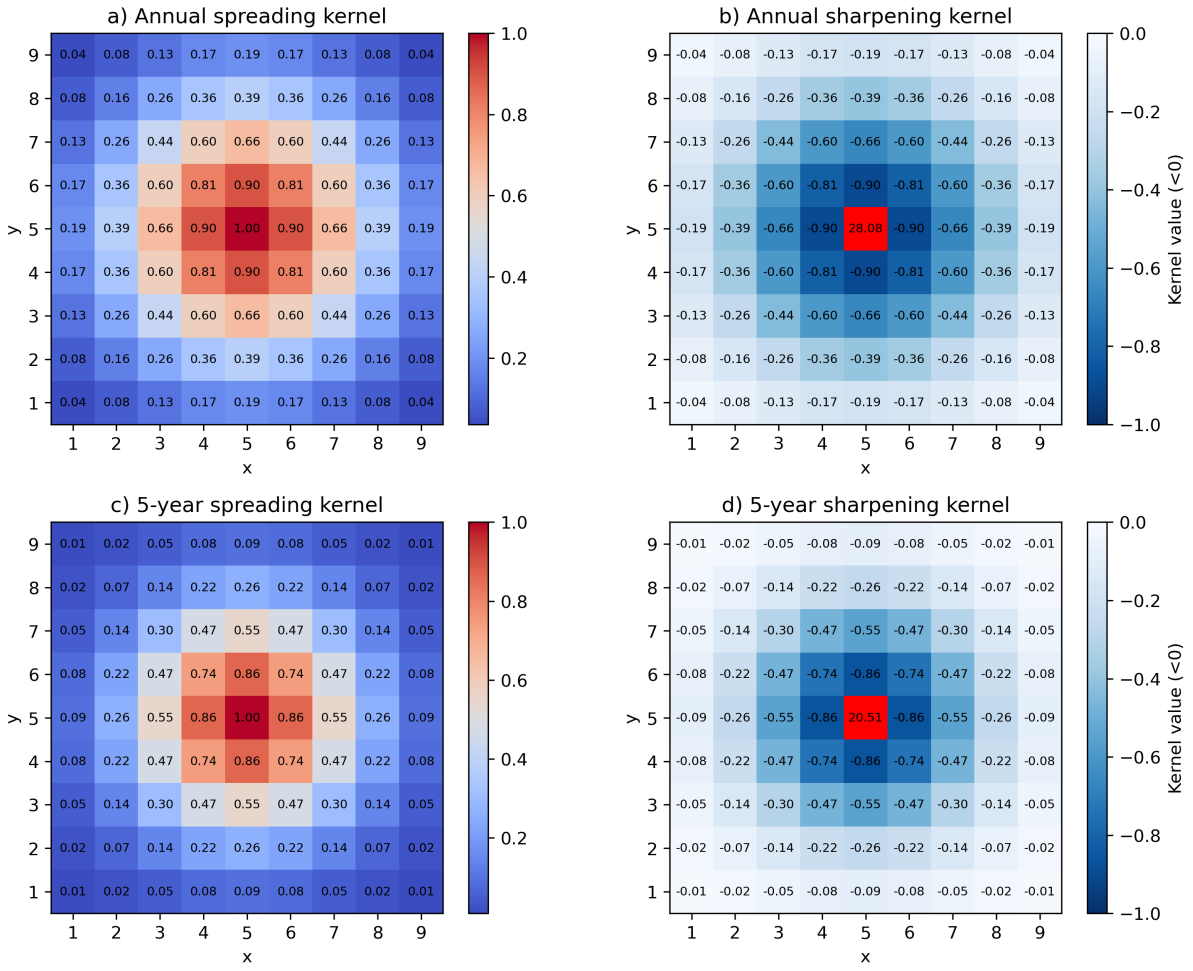

Figure S2. The spreading kernel derived from a) annual SO_2 emissions and c) five-year averaged SO_2 emissions. The sharpening kernels c) and d) are derived from their corresponded spreading kernels.

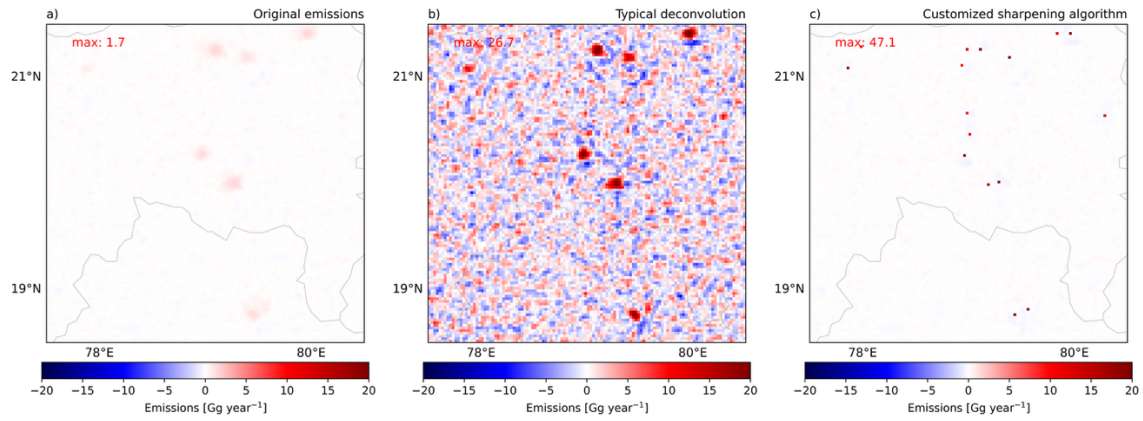

Figure S3. SO_2 emissions over a zoom-in region in India. a) Original SO_2 emissions. b) SO_2 emissions after the typical deconvolution. c) SO_2 emissions after customized sharpening algorithm (sharpening applied in descending order of emission).

S3. The spreading pattern derived from the model-based SO_2 emissions

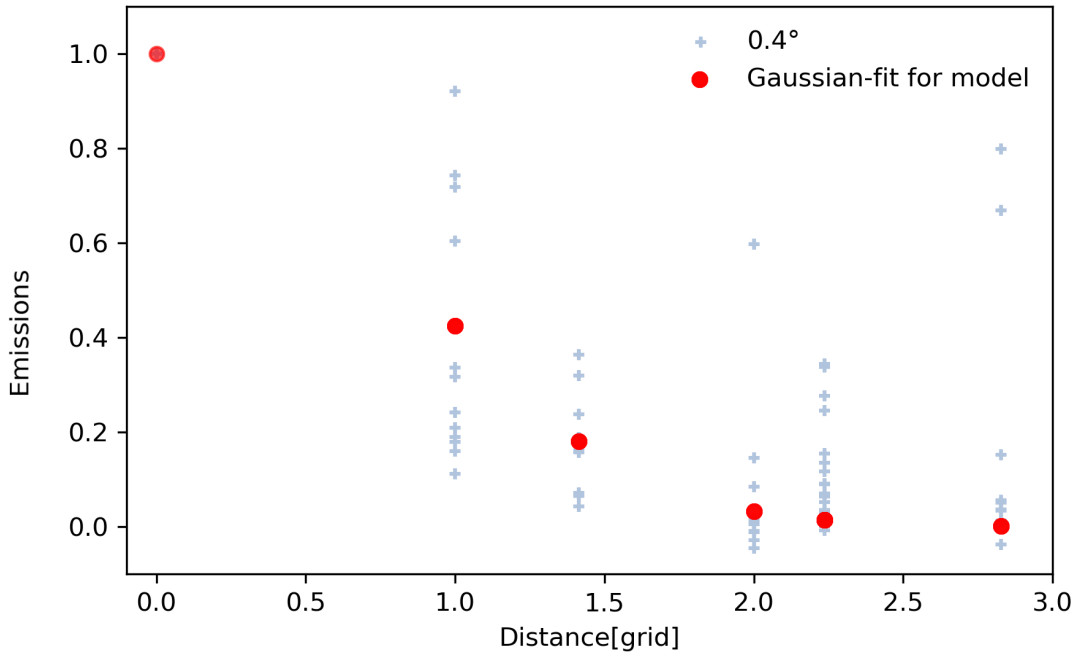

Figure S4. Variation of normalized SO_2 emissions with distance from the point source location, and the corresponding Gaussian-shaped fitting function with the sigma = 0.67. This emission is derived from the annual mean CAMS model results (0.4° × 0.4°). To avoid interference from nearby sources, we selected one isolated point source for this analysis. The point at (0,1) represents the location of the point emissions decrease to near zero within about two grid cells, so we define a 5 × 5 grid cell area centered on the point source as the emission spreading region.

S4. Point source improvement after sharpening.

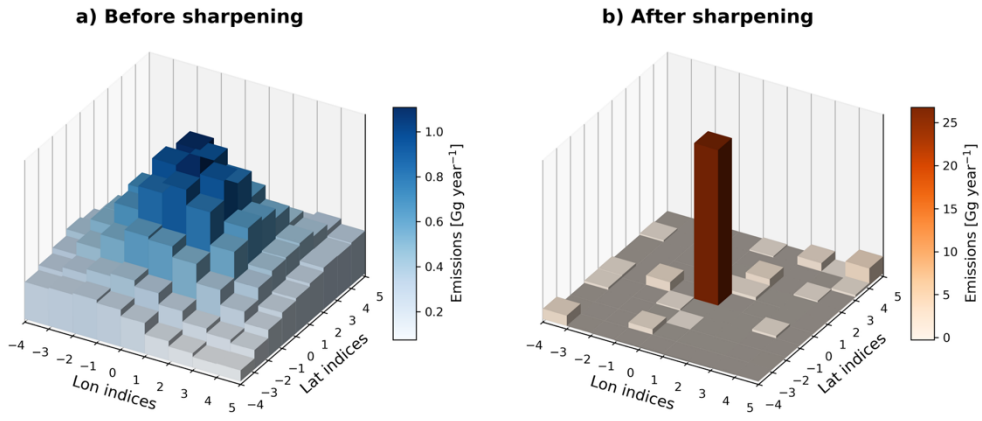

Figure S5. The SO_2 annual emission distribution a) before sharpening and b) after sharpening centered on a point source within a 9 × 9 grid cell area. This figure is based on the average of 38 selected point sources (See Table S2). The emissions before sharpening follows a 2D Gaussian pattern. The emission after sharpening is more concrete at the point source location and is enhanced approximately 28 times compared to the unsharpened case.

Table S2. Locations of selected SO_2 point source location used in Fig. S3

Name	Lat	Lon
INDRA GANDHI STPP	28,4849	76,3754
SURATGARH	29,179	74,0202
VALLUR ntpc/ntecl	13,2371	80,3023
UNCHAHAR	25,9131	81,3274
DAMODARAM SANJEEVAIAH	14,3444	80,1264
SAGARDIGHI TPP	24,3696	88,1046
YERMARUS TPP	16,2949	77,3568
RAYAL SEEMA	14,704	78,4577
BELLARY TPS	15,1932	76,7195
RAICHUR	16,3532	77,3422
AKALTARA TPP	21,9603	82,4091
K_GUDEM NEW	17,6219	80,6936
DADRI (NCTPP)	28,603	77,6078
LALITPUR TPP	24,7971	78,6463
PRYAGRAJ (BARA) TPP	25,196	81,6594
TALWANDI SABO	29,924	75,2372
SIMHADRI	17,591	83,0917
SINGRAULI STPS	24,1033	82,7068
FARAKKA STPS	24,772	87,894
CHHABRA TPS	24,6217	77,0357
MOUDA STPS	21,1797	79,3978
KAHALGAON	25,2349	87,2635
KORADI	21,2414	79,096
KUDGI	16,4994	75,8349
TAMNAR TPP	22,0987	83,4513
Shri Singaji MALWA TPP	22,0971	76,5317
KORBA STPS	22,3881	82,6858
R_GUNDEM STPS	18,7572	79,456
ANPARA	24,201	82,7891
CHANDRAPUR_Coal	20,0063	79,29
SIPAT STPS	22,13	82,293
RIHAND	24,027	82,7915
TALCHER STPS	21,0966	85,074
TIRORA TPP	21,4129	79,9671
SASAN UMPP	23,9784	82,6275
MUNDRA UMPP	22,8158	69,5281
MUNDRA TPP	22,823	69,5532
VINDH_CHAL STPS	24,0983	82,6719

Table S3 Locations of selected SO_2 point source location used in Fig. 7

Name	Lat	Lon
DURGAPUR STEEL TPS	23.58	87.2043
MARWA TPP	22.0708	82.6022
MEJIA TPS EXT	23.4639	87.1311
TUTICORIN JV	8.7603	78.1699
VIZAG TPP	17.5635	83.1382
BAKRESWAR	23.8285	87.4513
KAMALANGA	20.87	85.2671
MAITHON RB TPP	23.8209	86.76
TUTICORIN	8.7635	78.1753
JALLIPPA KAPURDI TPP	25.8888	71.3236
KAKATIYA TPP	18.3835	79.8265
UKAI_Coal	21.2093	73.5574
PARICHA	25.5124	78.7588
PARLI	18.8685	76.5254
ANAPARA "C"	24.2007	82.8
ANUPUR TPP	23.0655	81.7865
BARADARHA TPP	21.9114	83.1889
DERANG	21.1238	84.9843
MAHAN TPP	24.0077	82.4172
NORTH CHENNAI EXTENSION	13.245	80.3257
RAJIV GANDHI TPS HISAR	29.356	75.869
ROSA TPP PH - 1	27.818	79.936
SALAYA TPP	22.3049	69.7101
SINGARENI TPP	18.8372	79.5748
BHUSAWAL	21.0483	75.8425
KOTA	25.1712	75.8171
KOLAGHAT	22.4157	87.8713
VIJAYWADA	16.5984	80.537
BARH STPP II	25.4865	85.7452
KAWAI TPP	24.7773	76.737
MAHATMA GANDHI TPP	28.49	76.351
NIGRI	24.15	81.9045
PAINAMPURAM	14.3512	80.1431
SEMBCORP GAYATRI	14.351	80.1443
KORBA-WEST	22.4118	82.6888
K_KHEDA II	21.2818	79.116
MEJIA	23.4639	87.1311
SANJAY GANDHI	23.3026	81.0668
AMARAVATI TPP	21.0782	77.9009
RAIKHEDA	21.4499	81.8525

RAJPURA TPP	30.557	76.577
UCHPINDA TPP	21.8858	83.1215
NEYVELI ST II	11.5576	79.4417
WANAKBORI	22.8725	73.3588
INDRA GANDHI STPP	28.4849	76.3754
SURATGARH	29.179	74.0202
VALLUR ntpc/ntecl	13.2371	80.3023
UNCHAHAR	25.9131	81.3274
DAMODARAM SANJEEVAIAH	14.3444	80.1264
SAGARDIGHI TPP	24.3696	88.1046
YERMARUS TPP	16.2949	77.3568
RAYAL SEEMA	14.704	78.4577
BELLARY TPS	15.1932	76.7195
RAICHUR	16.3532	77.3422
AKALTARA TPP	21.9603	82.4091
K_GUDEM NEW	17.6219	80.6936
DADRI (NCTPP)	28.603	77.6078
LALITPUR TPP	24.7971	78.6463
PRYAGRAJ (BARA) TPP	25.196	81.6594
TALWANDI SABO	29.924	75.2372
SIMHADRI	17.591	83.0917
SINGRAULI STPS	24.1033	82.7068
FARAKKA STPS	24.772	87.894
CHHABRA TPS	24.6217	77.0357
MOUDA STPS	21.1797	79.3978
KAHALGAON	25.2349	87.2635
KORADI	21.2414	79.096
KUDGI	16.4994	75.8349
TAMNAR TPP	22.0987	83.4513
Shri Singaji MALWA TPP	22.0971	76.5317
KORBA STPS	22.3881	82.6858
R_GUNDEM STPS	18.7572	79.456
ANPARA	24.201	82.7891
CHANDRAPUR_Coal	20.0063	79.29
SIPAT STPS	22.13	82.293
RIHAND	24.027	82.7915
TALCHER STPS	21.0966	85.074
TIRORA TPP	21.4129	79.9671
SASAN UMPP	23.9784	82.6275
MUNDRA UMPP	22.8158	69.5281
MUNDRA TPP	22.823	69.5532
VINDH_CHAL STPS	24.0983	82.6719

S6. Noise level and detection threshold

The noise levels for one-year annual emissions and five-year averaged emissions are different. To quantify the noise, we selected a clean ocean region without SO_2 emissions (5°–18° N, 85°–90° E). The emission signal within this region was treated as noise. For the annual emissions, the frequency distribution of the noise in the selected clean region approximates a normal distribution with a standard deviation of $\sigma = 0.125$ Gg yr^{-1}. To avoid inflating the noise level, we define the noise threshold as three times σ (3σ), corresponding to 0.38 Gg yr^{-1} per grid cell. In our case, the sharpening procedure increases the signal in the central grid cell by approximately a factor of 28. Therefore, the detection threshold for the annual sharpened emission map is 10 Gg $year^{-1}$.For the five-year averaged emissions, σ is 0.06 Gg yr^{-1}, yielding a 3σ noise level of 0.17 Gg $year^{-1}$. The sharpening leads to an enhancement factor of approximately 20, resulting in a detection threshold of 3.4 Gg $year^{-1}$ for the five-year averaged emissions.

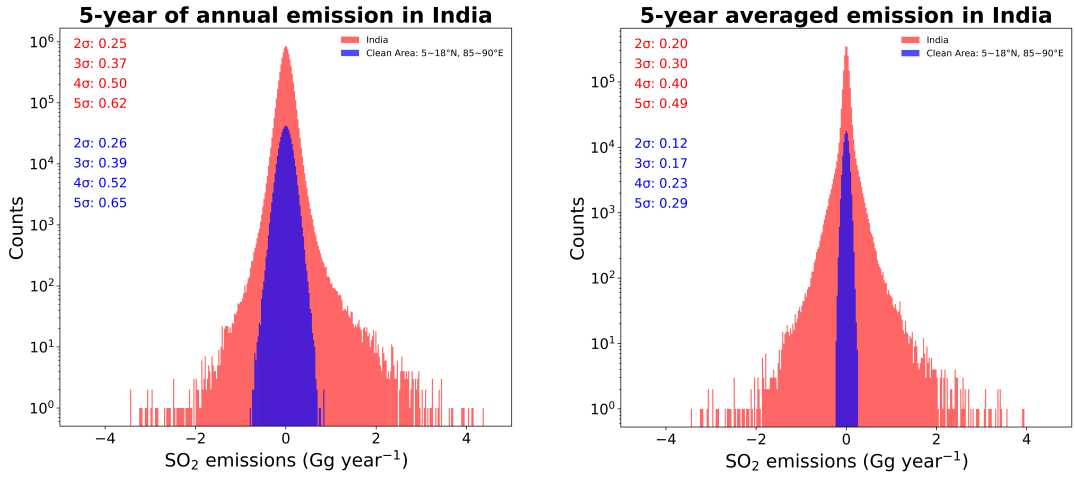

Figure S6. Histogram of the frequency of SO_2 emissions. The red bars represent the frequency of SO_2 emissions within the simulation domain. The blue bars denote the frequency of SO_2 emissions (or the noise) in the selected clean oceanic region (latitude: 5°N-18°N; longitude: 85°E-90°E). The left panel is derived from the annual emissions, and the right panel is derived from the five-year averaged emissions.